

## APPLICATION OF THE BOUNDARY ELEMENT METHOD TO THE COMPRESSIVE STRAIN-SOFTENING BEHAVIOUR OF CONCRETE

A. Carpinteri, F. Ciola, N. Pugno  
Politecnico di Torino, Department of Structural Engineering, Torino, Italy  
G. Ferrara, M. E. Gobbi  
ENEL-CRIS, Milano, Italy

### Abstract

In the present paper the compressive mechanical behaviour of quasi-brittle materials is analysed by means of experimental tests and by using an *ad hoc* boundary element algorithm for the numerical simulations.

The experimental analysis is carried out on specimens with three size-scales, three different slendernesses and two boundary conditions.

The numerical analysis was carried out by taking into account the initial random crack distribution, considering the mutual interaction, the crack-boundary interaction and the internal friction between the faces of the cracks.

The numerical simulations, in good agreement with the experimental results, highlight the characteristic strain-softening behaviour of quasi-brittle materials, and the influence of size-scale and slenderness on the structural response. By observing the evolution of the crack patterns, it is possible to emphasize, both experimentally and numerically, the transition from crushing collapse to splitting collapse by increasing the specimen slenderness, as well as the transition from ductile to brittle behaviour by increasing the specimen size-scale.

Key words: Concrete, compression, strain-softening, boundary elements.

## 1 Introduction

The study of the compressive mechanical behaviour of concrete, already analysed by several authors, does not present till today a complete and systematic treatment, even if many salient aspects have been already emphasized.

The most important of these aspects is constituted by the phenomenon of strain-softening that presents variable characteristics by varying the test conditions. There are in fact many parameters to be taken into account, and two are the most important: the slenderness of the specimen and the friction between the specimen and the loading platens.

The present investigation highlights these aspects experimentally and numerically. The experimental analysis was carried out at the ENEL-CRIS Laboratories in Milano (Ferrara and Gobbi, 1995) in the framework of the Round-Robin Test promoted by RILEM TC 148 SSC, whereas an *ad hoc* boundary element algorithm was implemented and utilized for the numerical simulations.

## 2 Experimental analysis

### 2.1 Materials and specimens

The experimental tests have been carried out on concrete specimens characterized by the following parameters:

- one quality of concrete (normal strength concrete);
- three specimen sizes: prisms with square bases of side 50 - 100 - 200 mm;
- three slendernesses ( $L/D$  equal to 0.5 - 1 - 2);
- two boundary conditions (with and without friction).

As regards the concrete quality, only one type of concrete was used with the following composition:

- 425 Portland cement with a batching of  $375 \text{ Kg/m}^3$ ;
- aggregates with the following size distribution:

0.125-0.25 mm	127 $\text{Kg/m}^3$ ;
0.25-0.5 mm	234 $\text{Kg/m}^3$ ;
0.5-1.0 mm	272 $\text{Kg/m}^3$ ;
1.0-2.0 mm	272 $\text{Kg/m}^3$ ;
2.0-4.0 mm	363 $\text{Kg/m}^3$ ;
4.0-8.0 mm	540 $\text{Kg/m}^3$ ;
- water to cement ratio equal to 0.5.

The casting procedure was the following. The concrete was poured in the moulds, and compacted on a vibration table for 30 seconds. Then, the specimens were kept in the moulds for two days, at 90% U.R. and under wet cloths. After demoulding, the specimens were placed in a fresh water basin at 20°C. Sawing of specimens was done at the age of 14 days.

It is important to emphasize that the specimens were not obtained directly; larger blocks were previously cast, from which the prisms have been afterwards sawn. At this regard, there is the correspondence shown in Table 1.

Table 1

block dimensions (mm)	specimen basis dimensions (mm)
100x100x500	prisms 50x50
150x150x600	prisms 100x100
200x200x600	prisms 150x150

The direction of loading in the compression test was perpendicular to the direction of casting, to remove the weak top layer that could lead to flexural stresses. All the specimens were cut by diamond grinding disks. Their bases in contact with the loading platens were ground flat by the flattening machine. After sawing, the specimens have been kept in the water basin for 28 days. At this age they were sealed in plastic bags and kept in a 90% U.R. chamber until the moment of testing. In order to guarantee the perfect contact between the loading platens and the specimens, a cement capping was performed before beginning the tests, at an age of 11 weeks.

## 2.2 Loading and recording system

One of the purposes of the present research is to determine the effect of frictional restraint between specimen and loading platens on the experimental response.

The two testing machines (of different stiffness and loading capacity) were equipped with rigid steel platens, i.e. without rotation capability. The rigid loading platens present the same square cross-section for prisms. The direct contact of the specimen with the loading platens produces friction conditions at the interface, since the concrete lateral expansion is not allowed. Among the various frictionless loading systems, the application of teflon interlayers between specimen and steel platens was chosen.

The measurement of the load, performed by a dynamometric cell, was directly transmitted to the acquisition station. The overall vertical displacement was measured with inductive displacement transducers with  $\pm 5$  mm of stroke and a sensitivity of 1.25 micrometers. The vertical transducers average, coming out of the station, served as feed-back signal in the closed-loop servocontrol. The loading rate was 1  $\mu\text{m/s}$ .

The disposal of the vertical transducers allows measurements including the deformation of the steel platens and of the teflon interlayers, in addition to the specimen deformation. To obtain the correct strain value, it was necessary to eliminate from the measurement the contributions of the two additional elements. In order to obtain the real value, the strain of cement capping was also to be eliminated.

### 3 Numerical analysis

#### 3.1 Computation Algorithm

To interpret the experimental data, a set of numerical simulations was carried out, by developing to this aim an *ad hoc* boundary element algorithm.

The numerical algorithm is based on the Superposition Principle and allows to represent the stress field in a finite plate with several cracks as the superposition of elementary cases (Fig. 1).

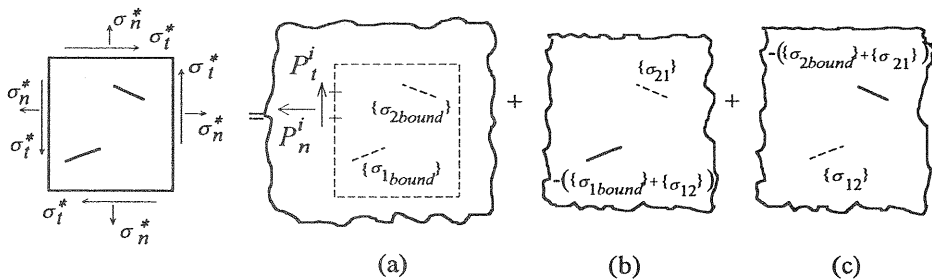


Fig.1. Schemes for the application of the Superposition Principle

Scheme (a) derives from the application of the Boundary Element Method (Crouch and Starfield, 1983; Brencich and Carpinteri, 1996); on the other hand, the analysis of the stress field in schemes (b) and (c) is made by referring to Sneddon (1969) formulation. This was also assumed by Yang (Yang and Liu, 1991; Carpinteri et al., 1996; Carpinteri and Yang,

1996, 1997a, 1997b) and provides the stress field as a function of normal and shearing stresses acting directly on the crack edges.

Using the Sneddon (1969) formulation and applying the Superposition Principle, a linear system may be written, the solution of which provides the normal and shearing stresses acting on the crack edges in the schemes (b) and (c). The determination of the stress-intensity factors  $K_I$  e  $K_{II}$  is made by considering the mutual interaction as well as the crack-boundary interaction. In addition, it is possible to take into account the internal friction between the faces of the crack. When compressive normal stresses act on the crack surfaces, friction shearing stresses  $\tau_f = \lambda\sigma$  appear, contrasting relative slippage ( $\lambda$  is the internal friction coefficient).

If shearing stresses are active on the crack, the effect of these is diminished by the friction shearing stresses. If  $|\tau| > |\lambda\sigma|$  the effective stress is:

$$\tau_{eff} = \tau \left( 1 - \frac{|\lambda\sigma|}{|\tau|} \right) \quad (1)$$

If  $|\tau| < |\lambda\sigma|$  then  $\tau_{eff} = 0$ . By using the concept of  $\tau_{eff}$ , it is possible to compute the stress-intensity factors taking into account the internal friction. The above formulation may be easily extrapolated to multicroaked geometries.

### 3.2 Numerical modelling

In order to study the experiments in a realistic way, it is impossible to leave out of consideration the random distribution of cracks initially present in the material. The internal damage develops over three different scale levels (micro-, meso- and macrocracks) and is present even before the loading process.

In connection with what has been written above, a structural scheme constituted by a finite plate with a random distribution of initial meso- and macrocracks is adopted in the numerical simulations. Starting from this geometry and using the above mentioned formulation, the stress field and the stress-intensity factors acting on each crack are calculated. Then, referring to the well-known maximum hoop stress criterion (Erdogan and Sih, 1963), for each crack tip an equivalent stress-intensity factor is defined as:

$$K_{eq} = \cos \frac{\theta}{2} \left[ K_I \cos^2 \frac{\theta}{2} - \frac{3}{2} K_{II} \sin \theta \right] \quad (2)$$

where  $\theta$  is the propagation angle, so that the crack with the highest  $K_{eq}$  can be determined. Comparing the highest  $K_{eq}$  with the critical value  $K_{IC}$ , the external load of crack propagation can be calculated.

The next step is to cause the crack to propagate by a finite amount only at the tip where it is more solicited. At this stage, we are faced with a new geometry, on which it is necessary to carry out a fresh analysis. The procedure is then iterated until the specimen completely collapses. In this way it is possible to follow the crack pattern evolution during the loading process, computing the critical stress at each step.

As regards the deformation response of the specimen, it is necessary to define a fundamental parameter represented by the global compliance. This is provided by two contributions: the former,  $C'$ , is spread and depends on the specimen dimensions and on the elastic modulus; the latter is due to the cracks and is called incremental compliance,  $C''$ . Both the compliances,  $C'$  and  $C''$ , vary during the loading simulation.

When the crack propagates, the variation in  $C''$  is governed by the well-known differential relation:

$$g_I = \frac{1}{2} F^2 \frac{\partial C''}{\partial a} = \frac{K_I^2}{E} + \frac{K_{II}^2}{E} \quad (3)$$

where  $F$  is the applied load.

As regards the compliance contribution due to the material elasticity, the constancy assumption for the material elastic modulus does not reflect the physical evolution of the phenomenon. In fact, during the loading process, the microcracks, approximately distributed in a uniform manner, grow in the material, so that their macroscopic effect is the progressive decay of bulk elasticity. This particular aspect plays a fundamental role in the real behaviour of the material.

In this work, as already made in previous studies (Sih and Madenci, 1983; Carpinteri and Sih, 1984; Carpinteri, 1986), the hypothesis is made that the decay of the elastic modulus depends on the energy absorbed by the material: the larger the energy absorbed, the lower the elastic modulus. This behaviour is approximated satisfactorily by a decreasing function of the form:

$$E^* = E \left( \frac{a}{W^\alpha} + b \right) \quad (4)$$

where  $E$  is the initial elastic modulus,  $E^*$  is the decayed elastic modulus,  $W$  is the strain energy density absorbed during the loading process,  $\alpha \cong 0.5$  and  $a$  and  $b$  are two constants determined from experimental data.

#### 4 Experimental results and numerical simulations

In this section, a comparison between the experimental results and the numerical simulations will be presented. The comparison regards the prismatic specimens with a square base (50x50, 100x100, 150x150 mm<sup>2</sup>) and with three different slendernesses (0.5, 1.0, 2.0), with and without friction between the specimen and the loading platens, for a total of eighteen cases.

The friction condition is represented by the direct contact between specimen and platens, since the shearing stresses at the interface arise in opposition to the lateral expansion of the specimen. From the computational point of view, this phenomenon is modelled by dividing the loaded boundaries in two parts and by imposing on each part a shearing stress directed inwards (Fig. 2).

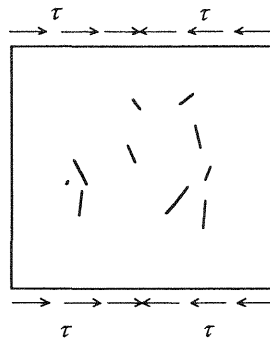


Fig. 2. Friction shearing stresses

On the other hand, the introduction of teflon layers between the specimen and the loading platens allows for the lateral expansion of the material; as a consequence, the shearing stresses at the interface become negligible (the friction coefficient is close to 0.01). In the related numerical simulations there is only the compressive normal stress.

Some experimental and numerical results are presented in Figures 3 to 8.

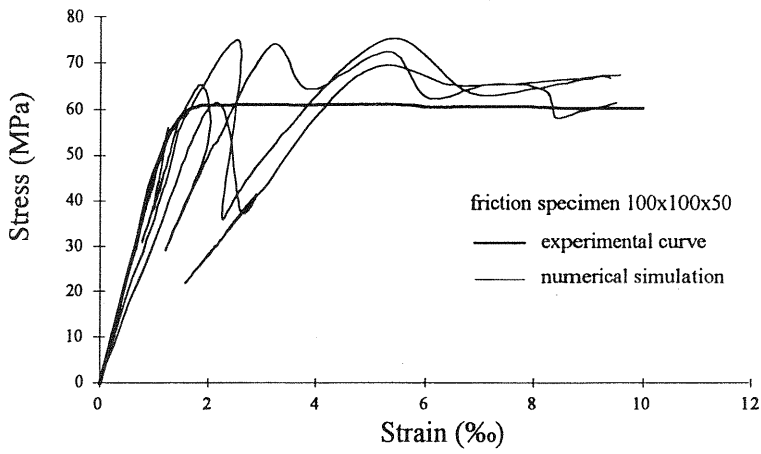


Fig. 3. Stress-Strain curves for the 100x100x50 specimen with friction

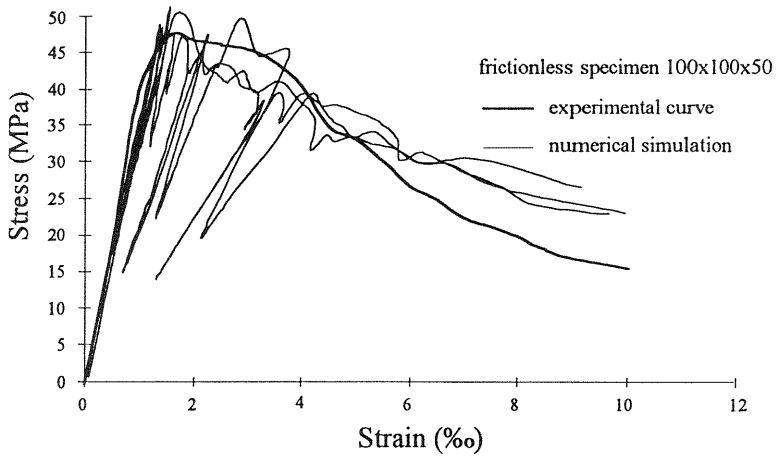


Fig. 4. Stress-Strain curves for the 100x100x50 specimen without friction

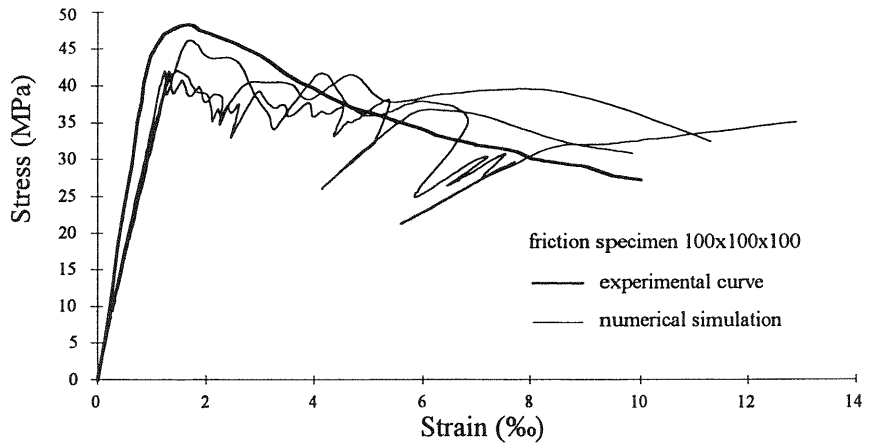


Fig. 5. Stress-Strain curves for the 100x100x100 specimen with friction

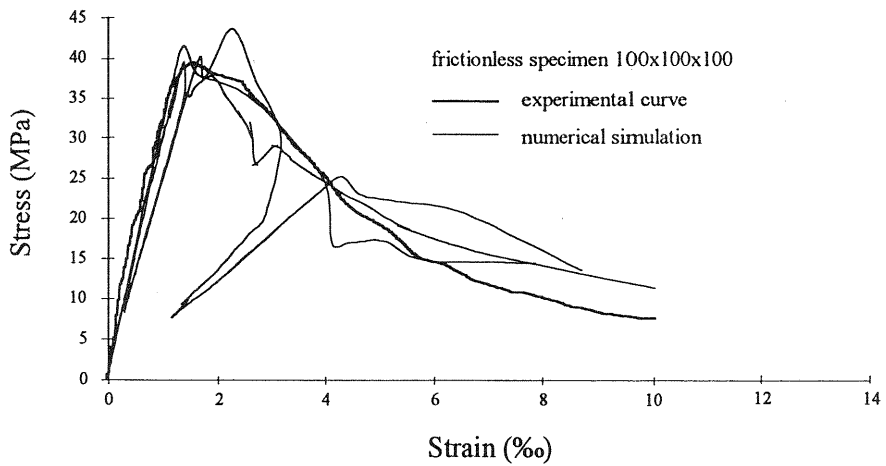


Fig. 6. Stress-Strain curves for the 100x100x100 specimen without friction

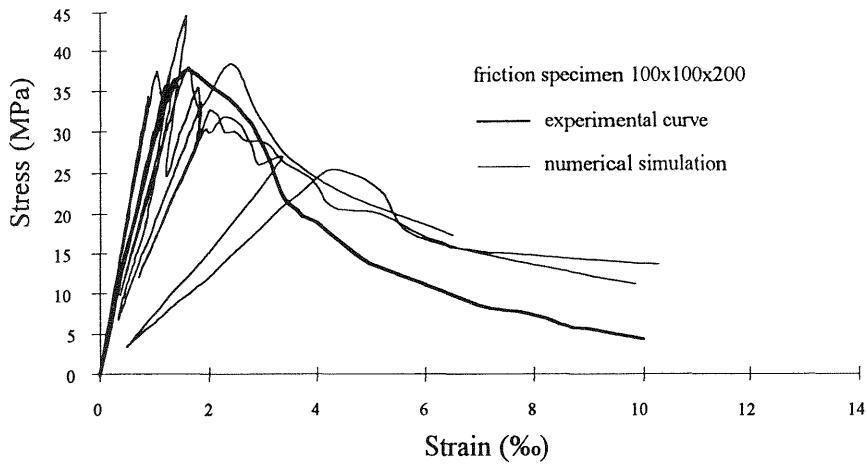


Fig. 7. Stress-Strain curves for the 100x100x200 specimen with friction

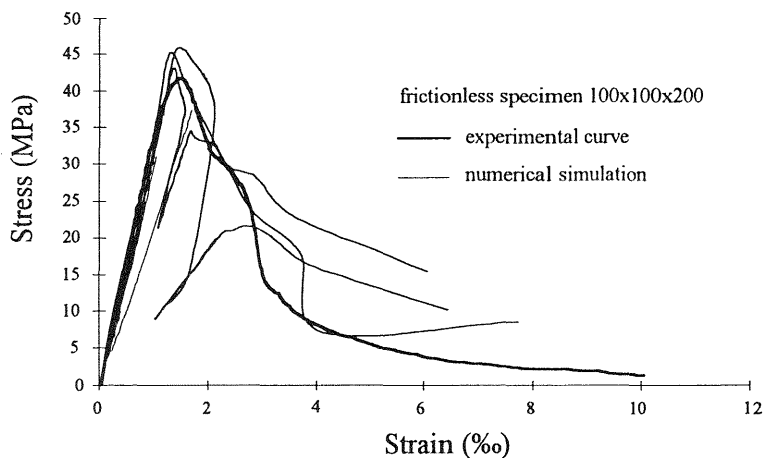


Fig. 8. Stress-Strain curves for the 100x100x200 specimen without friction

## 5 Discussion and conclusions

The analysis of the results presented in the paper shows a satisfactory correspondence between the numerical simulations and the experimental tests.

The cases in which the unavoidable differences are more evident are those related to small and stubby specimens with friction. These differences are due to the fact that, in these conditions, the real specimen

behaviour moves away from the idealized plate behaviour. The numerical model, however, gives good results in the other cases, confirming the validity of the theoretical assumptions on which it is based.

To this regard, it is important to emphasize the centrality of the cracking phenomenon in the structural response. Although the structural collapse is mainly governed by meso- and macrocracks, at the same time it is very important to take into account the widespread elastic decay due to the microcracks. It allows to capture the softening branch, which is typical of quasi-brittle materials and otherwise not reproducible.

If the stress-strain responses are considered, some interesting aspects arise, which were also shown in other studies (Van Mier, 1984; RILEM Report, 1997). First of all, it is important to highlight the friction influence. For all the geometries the following aspects clearly arise: in the friction cases there is a considerable variation in strength by varying the slenderness; the same trend is very mitigated or even absent in frictionless cases. As a matter of fact, the frictional shearing stresses acting at the interface produce triaxially-confined regions near the bases. In these regions, a compressive stress field is present. For small slendernesses, the confined regions include most of the specimen (Fig. 9). As a consequence, the maximum loading capacity is higher for stubby specimens (it is well-known that the triaxial compressive strength is usually larger than the uniaxial compressive strength). Hence it is possible to explain the variation in strength by varying the slenderness in the friction tests, and the absence of this phenomenon when the teflon layers are used.

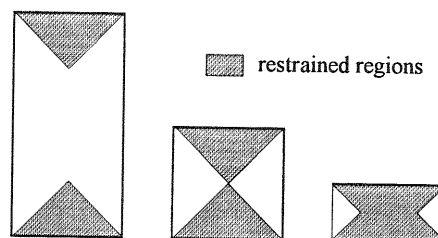


Fig. 9. Restrained regions in friction specimens

An additional important trend is represented by the ductility increase versus the specimen slenderness decrease. This trend, emerging in all the test results more or less clearly, is connected with and has a justification in the structural collapse schemes. When the slenderness decreases, a transition from *splitting* to *crushing* collapse occurs. Also the numerical simulations confirm the same aspect (Figs. 10 and 11).

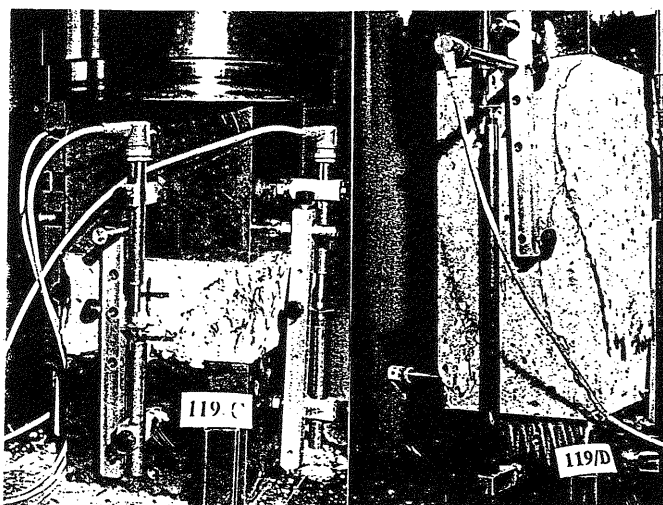


Fig. 10. Different experimental collapse characteristics

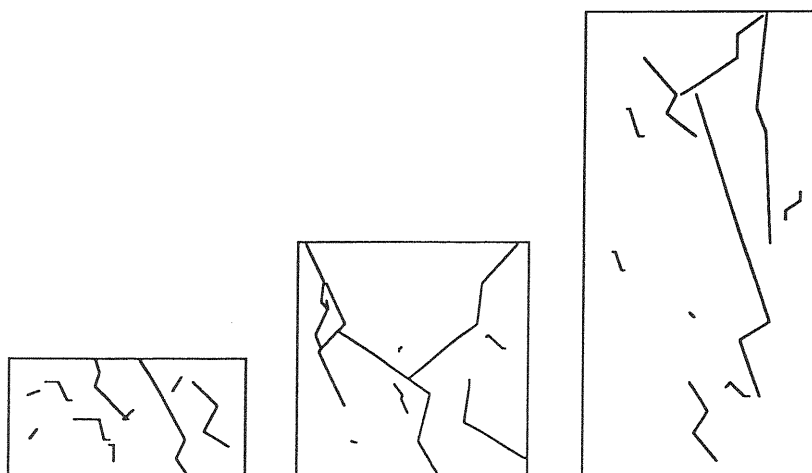


Fig. 11. Different numerical collapse schemes by varying the specimen slenderness

On the other hand, the *crushing* collapse, which is characterized by a multitude of microcracks (this phenomenon also occurs in the numerical simulations, in which  $E^*$  decays rapidly), is associated with a larger energy dissipation during rupture and therefore with a more ductile behaviour. On the contrary, the *splitting* collapse, which is characterized by a more localized rupture (this aspect is reflected also by the numerical

simulations), requires a smaller energy dissipation and then produces a more brittle behaviour.

## 6 Acknowledgements

The present research was carried out with the financial support of the Ministry of University and Scientific Research (MURST), the National Research Council (CNR) and the EC-TMC Contract N° ERBFMRXCT960062.

## 7 References

- Brenich, A. and Carpinteri, A. (1996) Interaction of a main crack with ordered distributions of microcracks: a numerical technique by displacement discontinuity boundary elements. **International Journal of Fracture**, 76, 373-389.
- Carpinteri, A. (1986) **Mechanical Damage and Crack Growth in Concrete**, Martinus Nijhoff Publishers, Dordrecht.
- Carpinteri, A. and Sih, G.C. (1984) Damage accumulation and crack growth in bilinear materials with softening: application of strain energy density theory. **Theoretical and Applied Fracture Mechanics**, 1, 145-160.
- Carpinteri, A. and Yang, G.P. (1996) Fractal dimension evolution of microcrack net in disordered materials. **Theoretical and Applied Fracture Mechanics**, 25, 73-81.
- Carpinteri, A. and Yang, G.P. (1997a) Damage process in finite sized brittle specimen with interacting microcracks. **Fracture & Fatigue of Engineering Materials & Structures**, 20, 1105-1115.
- Carpinteri, A. and Yang, G.P. (1997b) Size effects in brittle specimen with microcrack interaction. **Computers & Structures**, 63, 429-437.
- Carpinteri, A., Scavia, C and Yang, G.P. (1996) Microcrack propagation, coalescence and size effects in compression. **Engineering Fracture Mechanics**, 54, 335-347.

- Crouch, S.L. and Starfield, A.M. (1983) **Boundary Element Methods in Solid Mechanics**, George Allen and Unwin, London.
- Erdogan, F. and Sih, G.C. (1963) On the crack extension in plates under plane loading and transverse shear. **Journal of Basic Engineering**, 85, 519-527.
- Ferrara, G. and Gobbi, M.E. (1995) Strain softening of concrete under compression, **Report to RILEM Committee 148 SSC**, ENEL-CRIS Laboratory, Milano, Italy.
- Sih, G.C. and Madenci, E. (1983) Crack growth resistance characterized by the strain energy density function. **Engineering Fracture Mechanics**, 18, 1159-1171.
- Sneddon, N.I. and Lowengrub, M. (1969) **Crack Problems in The Classical Theory of Elasticity**, John Wiley & Sons, Inc.
- Strain softening of concrete in uniaxial compression (1997) Report of the Round Robin Test carried out by RILEM TC 148 SSC. **Materials & Structures**, 30, 195-209.
- Van Mier, J.G.M. (1984) Strain softening of concrete under multiaxial compression, **Ph. D. Thesis**, Eindhoven University of Technology, Eindhoven, the Netherlands.
- Yang, G.P. and Liu, X.L. (1991) Microcracks interaction in concrete. **Int. Symp. on Concrete Engineering**, Nanjing, China.